Ultrafast hydrogen migration in acetylene cation driven by non-adiabatic effects

Mohamed El-Amine Madjet, Zheng Li, and Oriol Vendrell

Citation: The Journal of Chemical Physics **138**, 094311 (2013); doi: 10.1063/1.4793215
View online: http://dx.doi.org/10.1063/1.4793215
View Table of Contents: http://scitation.aip.org/content/aip/journal/jcp/138/9?ver=pdfcov
Published by the AIP Publishing

Ultrafast hydrogen migration in acetylene cation driven by non-adiabatic effects

Mohamed El-Amine Madjet,[1,a)] Zheng Li,[1,2] and Oriol Vendrell[1,b)]
[1]*Center for Free-Electron Laser Science, DESY, Notkestrasse 85, D-22607 Hamburg, Germany*
[2]*Department of Physics, University of Hamburg, D-20355 Hamburg, Germany*

(Received 18 December 2012; accepted 7 February 2013; published online 5 March 2013)

Non-adiabatic dynamics of the acetylene cation is investigated using mixed quantum-classical dynamics based on trajectory surface hopping. To describe the non-adiabatic effects, two surface hopping methods are used, namely, Tully's fewest switches and Landau-Zener surface hopping. Similarities and differences between the results based on those two methods are discussed. We find that the photoionization of acetylene into the first excited state $A^2\Sigma_g^+$ drives the molecule from the linear structure to a trans-bent structure. Through a conical intersection the acetylene cation can relax back to either the ground state of acetylene or vinylidene. We conclude that hydrogen migration always takes place after non-radiative electronic relaxation to the ground state of the monocation. Based on the analysis of correlation functions we identify coherent oscillations between acetylene and vinylidene with a period of about 70 fs after the electronic relaxation. © *2013 American Institute of Physics*. [http://dx.doi.org/10.1063/1.4793215]

I. INTRODUCTION

Hydrogen migration is one of the most important molecular rearrangement processes in chemistry. Such reactions often proceed on a femtosecond time scale and involve changes in the electronic structure of the molecular system coupled to ultrafast atomic motions. The isomerization of acetylene to vinylidene represents a prototype of hydrogen migration reactions and as such has been extensively investigated both experimentally and theoretically.[1–6]

With the recent advent of accelerator-based laser sources in the extreme ultraviolet (XUV) regime and the ability to control pump-probe delay times with femtosecond precision, it is now possible to follow the dynamics of ionized molecules from the moment of ionization up to a few hundred femtoseconds.[1–3] What is interesting in acetylene is the decay mechanism of the first excited state $A^2\Sigma_g^+$. To explain the fast decay of this state, several processes were proposed in the literature (see more details in Ref. 4). Theoretically, Rosmus *et al*.[5] suggested an isomerization mechanism from acetylene to vinylidene to be the decay channel. In the framework of a vibronic-coupling model, Gillen *et al*.[6] investigated the dynamics and spectroscopy of acetylene cation in the $X^2\Pi_u$ and $A^2\Sigma_g^+$ states. They explained the short lifetime of $A^2\Sigma_g^+$ state in terms of an ultrafast internal-conversion process caused by a conical intersection of $A^2\Sigma_g^+$ with the $X^2\Pi_u$ state. In a recent experimental study,[3] it was shown that the rapid decay of the initially populated $A^2\Sigma_g^+$ state was due to an ultrafast isomerization process. In our previous study,[7] we found that hydrogen migration goes hand in hand with the non-radiative decay of the first excited state to the ground state of the monocation.

It is well known that the Born-Oppenheimer approximation, in which nuclei are assumed to evolve on isolated potential energy surfaces, breaks down in atomic configurations where adiabatic electronic states are energetically close to each other due to non-adiabatic interaction.[8] To account for these non-adiabatic effects, many computational algorithms have been developed. The most accurate method is based on a fully quantum treatment for electronic and nuclear motion. For high-dimensional systems or quantum systems featuring large amplitude motions and a complex dynamics, full quantum calculations become computationally very demanding or unfeasible. There, mixed quantum-classical approaches represent a good alternative for modeling non-adiabatic effects. In these semiclassical approaches, the nuclei are treated classically whereas the electrons are described quantum mechanically.

The Ehrenfest (mean-field) method represents the most common scheme for treating the interaction between the classical and the quantum subsystems. In this approach, the nuclei move on an averaged single potential energy surface (PES).[9] As the mean-field method generally yields a mixed state which in some cases leads to unphysical dynamics, several alternatives to Ehrenfest dynamics were proposed. In these alternative methods, the dynamics is propagated on an adiabatic PES, but non-adiabatic transitions between PESs are allowed. Trajectory surface hopping (TSH)[10] is one of the most used methods to study the dynamics of non-adiabatic processes.[11–15] In several occasions TSH methods have been compared to full quantum treatments and good agreement found.[23] The fewest-switches surface hopping algorithm (FSSH) proposed by Tully[16] is the most popular implementation of TSH. The implementation of the FSSH is relatively straightforward but it requires the on-the-fly computation of the non-adiabatic coupling vectors as well as the integration of the quantum amplitudes of the electronic states at every point of the classical trajectory. Another

a)mohamed.el.amine.madjet@cfel.de.
b)oriol.vendrell@cfel.de.

simple and widely used scheme is the Landau-Zener surface hopping method (LZSH), which computes the transition probabilities with the Landau-Zener formula.[12,13,18,19] The LZSH scheme takes the energy spacing between the electronic states as a critical judgment for the hopping event, whereas FSSH scheme put stresses on the relative populations of electronic states.

Recently, the FSSH approach based on the time-dependent density-functional theory was applied to study non-adiabatic dynamics.[14,15,17] The problem of the excess of coherence was addressed by several authors. Granucci *et al.*[20] proposed a method for correcting the excess of coherence in FSSH. Subotnik and Shenvi[21] proposed a prescription for decoherence correction to FSSH dynamics. Landry *et al.*[22] showed that implementing a decoherence correction in the FSSH algorithm leads to the recovery of Marcus theory in the calculation of transition rates between adiabatic electronic states within the spin-boson model. As will be discussed later, in the present work trajectories quickly leave the interaction region and almost never return to it. In this case, the traditional FSSH has been repeatedly known to work correctly.

In this paper, we present a study of the dynamics of acetylene molecule after outer-valence ionization by an XUV photon. We analyze the dynamics of the system in terms of time-correlation functions and find that hydrogen migration always occurs after non-radiative electronic decay, and that the system can coherently oscillate between acetylene and vinylidene-like structures after the electronic relaxation for a few hundred femtoseconds. In our previous study based on LZSH and Koopmans' PESs,[7] we established the connection between electronic relaxation and hydrogen migration. Based on those calculations we found out that hydrogen migration could take place on the excited state PES without electronic relaxation. Based on the complete active space self-consistent field (CASSCF) calculations presented in this paper, we find that the conical intersection happens earlier in the hydrogen migration coordinates and that the vinylidene structure in the excited state of the cation has a higher potential energy by more than 1 eV. Therefore, we determine that hydrogen migration cannot take place in the excited state and always involves electronic relaxation.

The paper is structured as follows. In Sec. II, we present an overview of LZSH and FSSH to keep the discussion self-contained and we also describe the electronic structure calculations. In Sec. III A, we provide a detailed discussion of the electronic structure of the acetylene cation and the main reaction paths comparing to previously existing benchmark results. In Sec. III B, we discuss the non-adiabatic dynamics and in Sec. IV we conclude and provide a prospect for future work.

II. METHODS AND COMPUTATIONAL DETAILS

In adiabatic representation, the time-dependent electronic wave function can be expanded as follows:

$$\Psi(\vec{r}, \vec{R}, t) = \sum_i c_i(t)\Phi_i(\vec{r}; \vec{R}). \tag{2.1}$$

The expansion coefficients $c_i(t)$ are determined by propagating the time-dependent Schrödinger equation (TDSE)

$$i\hbar\frac{dc_j(t)}{dt} = \sum_i c_i(t)[H_{ji} - i\hbar\dot{\vec{R}}\cdot\vec{d}_{ji}], \tag{2.2}$$

where $\vec{d}_{ij}$ is the non-adiabatic (NAC) vector. In the adiabatic representation the Hamiltonian matrix H_{ji} is diagonal and Eq. (2.2) is simplified to

$$i\hbar\frac{dc_j(t)}{dt} = c_j(t)E_j - i\hbar\sum_i c_i\dot{\vec{R}}\cdot\vec{d}_{ji}. \tag{2.3}$$

The FSSH scheme requires the computation of the NAC coupling term between two electronic states i and j:

$$\dot{\vec{R}}\cdot\vec{d}_{ij} = \sigma_{ij} = \dot{\vec{R}}\langle\Phi_i(\vec{r}; \vec{R}(t)) \mid \vec{\nabla}_{\vec{R}}\Phi_j(\vec{r}; \vec{R}(t))\rangle. \tag{2.4}$$

The NAC coupling term σ_{ij} can be approximated by the finite difference,[25,26]

$$\sigma_{ij}(t + \Delta/2) = \frac{1}{2\Delta}\Big[\langle\Phi_i(\vec{r}; \vec{R}(t)) \mid \Phi_j(\vec{r}; \vec{R}(t + \Delta))\rangle - \langle\Phi_i(\vec{r}; \vec{R}(t + \Delta)) \mid \Phi_j(\vec{r}; \vec{R}(t))\rangle\Big]. \tag{2.5}$$

The hopping probability from state i to j is as follows:[16]

$$P_{ij} = -2\int_t^{t+\tau} d\tau\frac{\Re[c_j(\tau)c_i(\tau)^*\sigma_{ji}(\tau)]}{c_i(\tau)c_i^*(\tau)}. \tag{2.6}$$

In order to calculate the hopping probability P_{ij}, the coefficients c_i are obtained by numerical integration of the differential equation (Eq. (2.3)). The integration of the classical equations is done by using the velocity Verlet algorithm.[24] The NAC σ_{ij} is expressed in terms of the overlap between the wave functions at t and $t + \Delta$. The RASSI module contained in MOLCAS was used to compute overlap integrals between CASSCF wavefunctions necessary for the numerical estimation of the non-adiabatic couplings. The NAC term is calculated only at the midpoint (see Eq. (2.5)) between the two time steps for the nuclear dynamics, therefore in the interval $[t, t + \Delta/2]$ the NAC is linearly interpolated and linearly extrapolated in the interval $[t + \Delta/2, t + \Delta]$. For the propagation of the dynamics, the energies, gradients, and NACs are calculated on-the-fly. In this calculation, it is necessary to discard unphysical negative values for the probability.[27] Therefore, the final transition probability is defined as

$$g_{ij} = \max(P_{ij}, 0). \tag{2.7}$$

A random number ξ is generated ($0 \le \xi \le 1$) and at each time step and a hop from the state i to the state k is performed if $\sum_{j=1}^{k} g_{ij} < \xi < \sum_{j=1}^{k+1} g_{ij}$. After a hop, the nuclear trajectories evolve adiabatically on the state k. More details about recent implementations of the FSSH method can be found in Refs. 17 and 27–29. For the main methodological aspects of the TSH approach and its main applications see the recent review paper from Barbatti.[30]

There exists a simpler method for calculating the transition probability as compared to Eq. (2.6). This method is based on the Landau-Zener theory where the transition probability between the adiabatic states i and j is determined by

the local geometry of the PES:[12,31,32]

$$P_{ij}^{\mathrm{LZ}} = \exp\left(-2\pi \frac{(\Delta E_{ij})^2}{\hbar|\dot{\vec{R}} \cdot \vec{\nabla}(\Delta \tilde{E}_{ij})|}\right), \tag{2.8}$$

where ΔE_{ij} represents the energy difference between the two adiabatic states i and j and $\vec{\nabla}\Delta(\tilde{E}_{ij})$ is the gradient of the diabatic energy difference. Therefore, one needs at least three gradient calculations per time step in the LZSH implementation corresponding to the current state and the two closer energy eigenstates. On the other hand, for the FSSH scheme we need to evaluate NAC elements but we only need to compute the gradient for the state on which the dynamics is propagated which leads to a slightly more efficient method in most cases.

The term in the denominator of the exponent is evaluated as the maximum change in the adiabatic energy difference as the avoided crossing is approached.[32] By using a two state model with a constant coupling, it is easy to show that at all points the slope difference of the adiabatic energies is smaller than the slope difference of the diabatic energies. Therefore, near the avoided crossing, the gradient of the diabatic energy difference could be estimated from the maximum value of the gradient of the adiabatic energy difference. The transition probability is maximized for a minimum energy gap and/or for the largest gradient of the energy difference. This shows that the LZSH theory takes full advantage of the local geometry of the PESs for efficiently computing the transition probabilities. In the present work, only when the energy gap ΔE_{ij} is less than a given threshold (0.1 a.u. in the present study) the transition probability is computed and compared to a uniformly generated random number in the range [0,1] to decide whether a hopping event is taken. The implementation we used here for the Landau-Zener approach closely follows that of Jones *et al.*[32] In our implementation of Landau-Zener and fewest-switches schemes, the momentum of the nuclei are corrected immediately after the hopping along the direction of the gradient difference vector $\vec{n}$ as proposed in Refs. 33 and 34.

The phase space initial conditions for the trajectories were sampled from a Boltzmann distribution on the ground electronic state of the neutral system. The effect of the sampling temperature will be discussed later. The generated initial conditions were used to start every trajectory on the cationic states at $t = 0$. State-averaged CASSCF calculations with equal weights were used for computing the required energies, gradients and the NAC. The maximum simulation time is 400 fs for each trajectory and the nuclear integration time step is 0.2 fs while the electronic integration time step is 0.02 fs. A total of 100 trajectories were calculated. The impact of the user-defined parameters and approximations, such as classical and quantum integration time steps and hopping algorithms, used for non-adiabatic excited state molecular dynamics simulation can be found in a recent paper by Nelson *et al.*[35]

In the ground state, neutral acetylene has a linear structure and is described by the following electronic configuration $1\sigma_g^2\ 1\sigma_u^2\ 2\sigma_g^2\ 2\sigma_u^2\ 3\sigma_g^2\ 1\pi_u^4$. Removal of an electron from π_u, $3\sigma_g$, $2\sigma_u$, and $2\sigma_g$ leads to the cationic states, $X^2\Pi_u$, $A^2\Sigma_g^+$, $B^2\Sigma_u^+$, and $C^2\Sigma_g^+$, respectively. The molecular term symbols refer to the linear structure. In the text we sometimes refer to D_0 and D_1 as the two states corresponding to the doubly degenerate $X^2\Pi_u$ state, and to D_2 as the state corresponding to $A^2\Sigma_g^+$. Photoionization of the acetylene molecule was addressed theoretically by many authors. Wells *et al.*[36] used the multichannel scattering methodology to perform the calculation for the outer valence photoionization leading to the first four states of the acetylene monocation. Fronzoni *et al.*[37] applied the time-dependent density functional theory to study the valence and core photoionization dynamics of acetylene. Very recently, Douguet *et al.*[38] reported *ab initio* calculations on valence photoionization of the acetylene monocation in its ground and first excited states by using the complex Kohn variational method. Experimentally, the photoionization of acetylene molecule was studied by Cooper *et al.*[39] and by Mackie *et al.*[40] In the present study the ionization process is not explicitly considered. We assume that at $t = 0$, acetylene has been ionized to a cationic eigenstate by photoionization, from which the ultrafast dynamics initiates.

Mixed quantum classical Landau-Zener and a fewest-switches trajectory surface hopping algorithms are implemented into the Quantum Dynamics Tool Kit (QDTK).[41] Our code is interfaced to the electronic structure package MOLCAS.[42]

III. RESULTS AND DISCUSSION

A. Electronic structure and potential energy surface cuts

In this paper our aim is not to provide high level electronic structure calculations for the description of the ground and excited state properties of acetylene. Such calculations exist already in the literature.[43–52] Our focus is on the dynamics of acetylene that follows after an outer valence ionization. Given the large computational effort associated with the dynamics calculations, it is necessary to find a balance between accuracy and the simulation cost. Therefore, the choice of the active space is crucial for dynamics simulations. In fact, a large active space leads to longer simulation time whereas a smaller one will not be able to describe the dynamics correctly and may also lead to energy conservation problems. For all dynamics simulations, the active space is composed of nine electrons in eight orbitals, denoted as CAS(9,8). To perform the integration the relevant NACs were obtained by using Eq. (2.5). In order to check the quality of the electronic structure calculations used for the propagation of the dynamics, it will be useful to compare our results for the PESs with other published works based on similar or more accurate electronic structure calculations. More precisely we will first compare our PESs for the cis-bending path, trans-bending path, and the hydrogen migration path with those published in Refs. 45 and 46.

The geometry optimization of the acetylene monocation in the ground state, using CAS(9,8)/6-31G* level of theory, leads to linear geometry with the C–C and C–H bond lengths computed to be 1.27 and 1.07 Å, respectively. The C–C and C–H bond lengths of the optimized geometry of neutral acetylene are 1.22 and 1.06 Å, respectively. For the monocation, the C–C bond distance is longer by 0.05 Å than in the

TABLE I. Basis set dependence of the optimized geometry parameters for the first excited state of the acetylene cation computed at the CAS(9,8) level of theory. E_X represents the energy difference between the minimum of the potential surface of the $A^2\Sigma_g^+$ state and the ground state energy of the monocation. ϵ_X is the vertical excitation energy.

Basis set	E_X (eV)	ϵ_X (eV)	α (deg)	R_{CC} (Å)	R_{CH} (Å)
6-31G*	4.92	5.80	107.0	1.31	1.15
VDZ	4.36	6.83	111.4	1.33	1.18
VDZP	4.37	6.74	104.3	1.32	1.17
VTZP	4.86	5.89	104.21	1.31	1.16
VQZP	4.87	5.89	104.3	1.31	1.16

neutral acetylene. This behavior is expected as the ground state of the cation is obtained when removing an electron from the least bonding orbital which leads to weakening the C–C bond. The geometry for the first excited state was optimized at the CAS(9,8) level using different basis sets. The ANO-L-VDZ and ANO-L-VXZP (X = D, T, and Q) basis sets were used and the 6-31G* is given for comparison. The obtained results are shown in the Table I. Compared to the ground state, the C–C and C–H bonds for the $A^2\Sigma_g^+$ state are elongated. The optimized structure is a trans-bent geometry for the cation in the first excited state. Using higher basis sets leads to shortening the R_{CC} and R_{CH} bond distances. For the propagation of the dynamics we used the CAS(9,8)/6-31G*. This level of theory leads to $R_{CC} = 1.31$ Å, $R_{CH} = 1.15$ Å, and the C–C–H angle $\alpha = 107.0^\circ$. Our computed transition energy E_X (4.92 eV) at the CAS(9,8)/6-31G* level of theory is slightly higher than the one computed at the multi-reference configuration interaction (MRCI) level of theory (4.79 eV).[45] Also our computed vertical excitation energy computed at the CAS(9,8)/6-31G* level of theory is in good agreement with the MRCI value reported in Ref. 45.

In Figure 1 the potential energy cuts for the first five states of the acetylene monocation are shown, along the cis-bending path, as a function of the CCH angle while other geometric parameters are fixed at their ground state equilibrium values. We should mention that all the energies given in the PES cuts are given relative to the CASSCF energy of the ground state of the monocation. The states D_0 and D_1 are the two components splitting from the doubly degenerate ground state $X^2\Pi_u$ which is created by removing an electron from the highest occupied molecular orbital (HOMO). Similarly, the states D_2 and D_4 correspond to the first and second excited states of the monocation $A^2\Sigma_g^+$ and $B^2\Sigma_u^+$, respectively. However, the state D_3 has two-holes one-particle (2h-1p) state character. The D_2 and D_3 states are showing strong correlation going beyond the linear geometry. Therefore, a strong coupling and mixing between those two states are expected during the dynamics. In fact, we found that at shorter times the D_3 state get populated nearly up to 20%. Our results for the PESs along the cis-bending path are in good agreement with the results reported in Fig. 1 of Ref. 46 and also with those reported by Chambaud *et al.*[45] and shown in the present figure by filled circles. We note that the small differences seen between our results and those reported in Ref. 45 are due to the use of different basis sets and different active space.

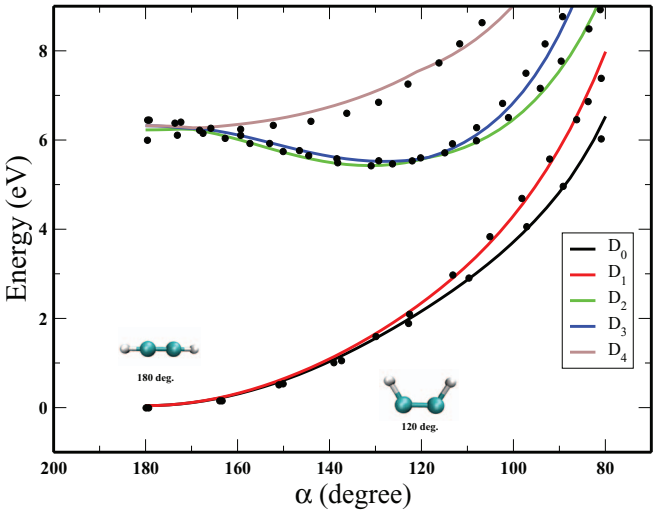

FIG. 1. Potential energy cuts along the cis-bending path as a function of the C–C–H angle (α). The R_{CC} and R_{CH} distances were kept fixed to 1.27 Å and 1.07 Å, respectively. Those bond lengths correspond to the optimized parameters for the acetylene cation in the ground state. All the energies given in the PES cuts are given relative to the CASSCF energy of the ground state of the monocation. The geometries of the molecule are shown at two different angles. The circles represent the CASSCF results from Ref. 45.

Figure 2 shows the potential energy cuts along the trans-bending path for the first five electronic states computed as a function of the CCH angle and where the C–C and C–H bond lengths are kept fixed to the equilibrium values of the first excited state, 1.31 and 1.15 Å, respectively. Along the trans-bending path, the potential of the cationic state $X^2\Pi_u$ is split in two components (D_0 and D_1). For the three lowest states, two conical intersections between the potential energy surfaces are found at around $\alpha = 98^\circ$ and 85° in good agreement with the finding reported in Ref. 45. The structure of the molecule at the first crossing is similar to the equilibrium geometry of the monocation in the $A^2\Sigma_g^+$ state. This means that if the system is prepared in the first excited state, the dynamics can evolve without any barrier to the first crossing region from where it can decay to the ground state. Our computed value for the energy difference between the minimum of the PES of the first excited state and that of the ground state (in the linear geometry) computed with 6-31G* basis set is 4.92 eV, larger by about 0.2 eV than the value reported in Ref. 53. Our results for the PESs along the trans-bending path shown in Figure 2 are in good agreement with those reported in Figure 3 of Ref. 45 and shown in our figure by filled circles.

Starting in the first region of conical intersection between the D_2 and D_1 states for the trans-bending path, and by moving one hydrogen atom around a fixed CCH structure (as done in Ref. 45), a barrierless path for the in-plane isomerization is found. The resulting PESs for such hydrogen migration path are plotted as a function of the angle (θ) in Figure 3. As one can see, the first excited state can immediately decay to the lower state D_1 on which the trajectory can evolve to the next crossing region located at an angle of about 78°. From there, there are two possibilities, decay to D_0 and stay in acetylene-like structures (for $\theta < 80^\circ$) or decay and evolve on vinylidene-like structures (for $\theta > 80^\circ$). We have also

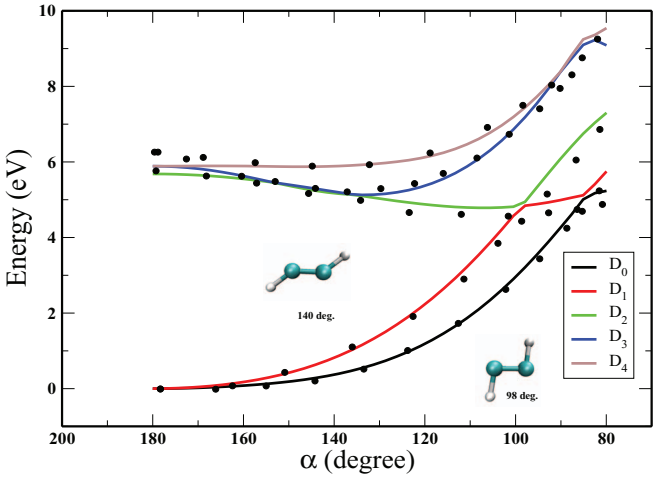

FIG. 2. Potential energy cuts along the trans-bending path as a function of the C–C–H angle (α), the R_{CC} and R_{CH} distances were kept fixed to 1.31 Å and 1.15 Å, respectively. The geometries of the molecule are shown at two different angles. The circles represent the CASSCF results from Ref. 45.

computed the hydrogen migration path at the CASPT2 level and good agreement was found between the CASSCF PESs (when shifted by a constant) and CASPT2 PESs specially for the three lowest electronic states of the cation. It is evident that the one-dimensional PES shown in Figure 3 cannot capture the full dynamics of isomerization which is in principle multi-dimensional, but it can be useful in understanding the competition process between the electronic decay to the ground state of acetylene-like structures and the decay process followed by isomerization.

In what follows, all the dynamics calculations are performed at the CAS(9,8)/6-31G* level of theory where nine electrons are included into the calculation with eight orbitals and averaged over 4 states.

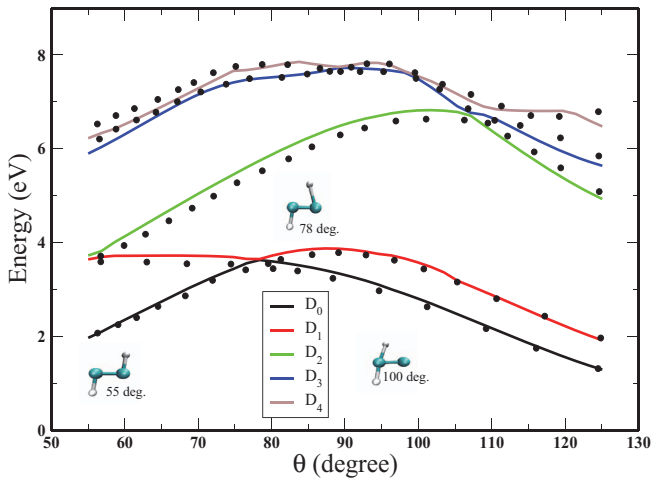

FIG. 3. Potential energy cuts for the in-plane hydrogen migration, where the R_{CC} and R_{CH} distances were kept fixed to 1.31 Å and 1.15 Å, respectively. One of the C–C–H angle is kept fix at 98°. The PES cuts are shown as a function of the angle of the second hydrogen relative to the center of the CC bond. The distance from the center of the CC bond to the hydrogen is also kept fixed. The geometries of the molecule are shown at three different angles. The circles represent the CASSCF results from Ref. 45, those results are shifted by a constant.

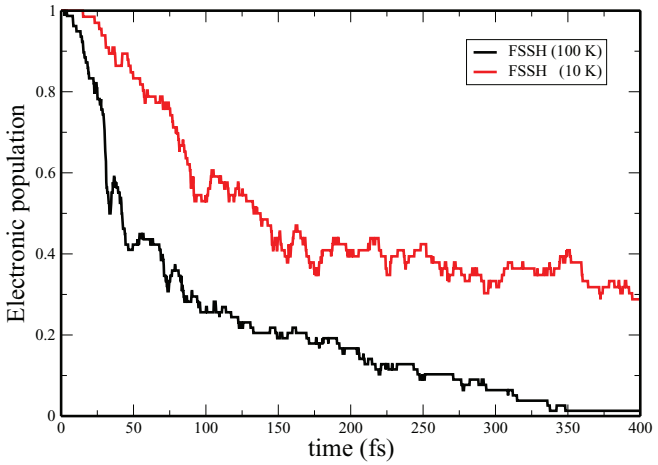

FIG. 4. Time evolution of the electronic population of first excited state $A^2\Sigma_g^+$ computed at two different sampling temperatures and using FSSH method.

B. Non-adiabatic dynamics

The initial conditions for the ensemble of TSH trajectories are sampled from a Boltzmann distribution. From experiments conducted in molecular beams the temperature of the molecules is unclear, but most probably below 100 K. In a classical dynamics study of the infrared spectroscopy of the Zundel cation it was shown that a temperature of 100 K was able to recover spectral features previously seen in full quantum studies.[54] Therefore, we sample from two initial temperatures, 10 K and 100 K. The calculations at 10 K serve mostly to compare the performance of LZSH and FSSH because a more compact set of initial conditions means that differences can be better understood in terms of the different assumptions of the approaches. The discussion of the ultrafast dynamics is then based on the calculations at 10 K and 100 K using FSSH. As discussed later, these two sets of calculations agree in all important mechanistic aspects and we believe that they enclose the results that would have been obtained from sampling a Wigner distribution of the ground vibrational state of the system.

The time evolution of the electronic population of the $A^2\Sigma_g^+$ states for initial preparation of the acetylene cation in the $A^2\Sigma_g^+$ state and computed using FSSH method is shown in Figure 4. During the first tens of femtoseconds, the electronic population remains essentially in the initial $A^2\Sigma_g^+$ state. Once the conical intersection is reached, ultrafast population decay of the $A^2\Sigma_g^+$ into the ground state takes place. The decay of the electronic population for the sampling temperature T = 100 K is faster than for T = 10 K. For the higher sampling temperature and already at 50 fs, half of the electronic population is transferred from the first excited state to the lower ground state. At 350 fs, 98% of the electronic population had decayed to the ground state. It is interesting to note that in the quantum dynamical study of Gillen *et al.*[6] the final population of the $A^2\Sigma_g^+$ state was about 20%, which is a value enclosed by our two sampling temperatures.

A comparison between the vinylidene fraction computed at two sampling temperatures and using the FSSH method is shown in Figure 5. For T = 100 K, the isomerization process

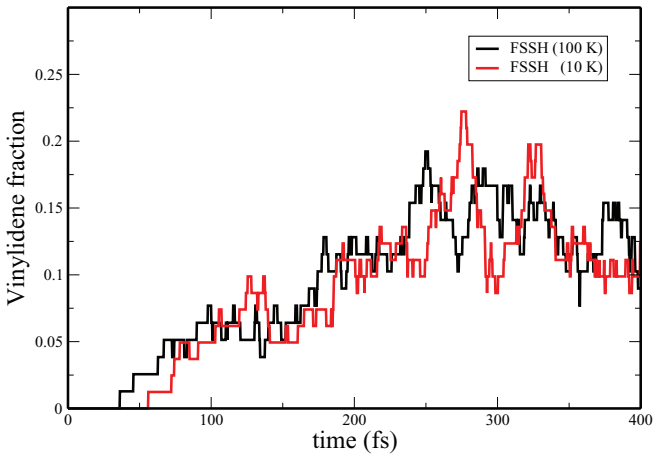

FIG. 5. Time evolution of the vinylidene fraction when starting from the first excited state $A^2\Sigma_g^+$. Results based on FSSH method are shown at two sampling temperatures. For both sampling temperatures, the maximum standard deviation is 0.045.

happens earlier than for T = 10 K. The vinylidene fraction computed at two different sampling temperatures are in good agreement and they present similar oscillations but with a relative shift respect to each other. It is maybe worth mentioning that most of the trajectories undergo isomerization at a later time after the electronic decay had occurred. After ionization into the $A^2\Sigma_g^+$ state, a rapid increase is found for the kinetic energy in the first 200 fs (data not shown here). After 200 fs the kinetic energy reaches a plateau value of about 1.9 eV. This increase in the kinetic energy is of course due to the conversion of potential energy to kinetic energy after the electronic decay to the ground state. It has been known that the isomerization from vinylidene cation to acetylene cation has a barrier height less than 0.6 eV.[52] This means that after the isomerization from acetylene to vinylidene, the molecule in a vinylidene structure has enough available energy to go back to acetylene-like structures. This recurrence effect is reflected by oscillations in the structure of the vinylidene fraction. This oscillatory behavior, which is not a quantum phenomenon, corresponds to oscillations of the trajectories between acetylene and vinylidene-like structures. This is a purely classical effect in which many trajectories evolve coherently and have not yet dephased from one another. As will be discussed later, similar oscillations can also be seen in the correlation functions. The issue of quantum or classical coherence was addressed very recently by Miller.[55] To investigate the correlation between the electronic decay (labeled as ed) and isomerization process (labeled as iso) let us define the following quantities for a given trajectory. First for the electronic decay we define

$$g_{\mathrm{ed}}(t) = \begin{cases} 1 & \text{if } D_2 \text{ decayed to } D_1 \text{ or } D_0 \\ 0 & \text{otherwise} \end{cases}, \tag{3.1}$$

and for the isomerization process we use

$$g_{\mathrm{iso}}(t) = \begin{cases} 1 & \text{if vinylidene-like structure} \\ 0 & \text{otherwise} \end{cases}. \tag{3.2}$$

Vinylidene configurations are defined here as those in which both hydrogens are found at the same side with respect to the imaginary plane intersecting the midpoint of the CC bond and

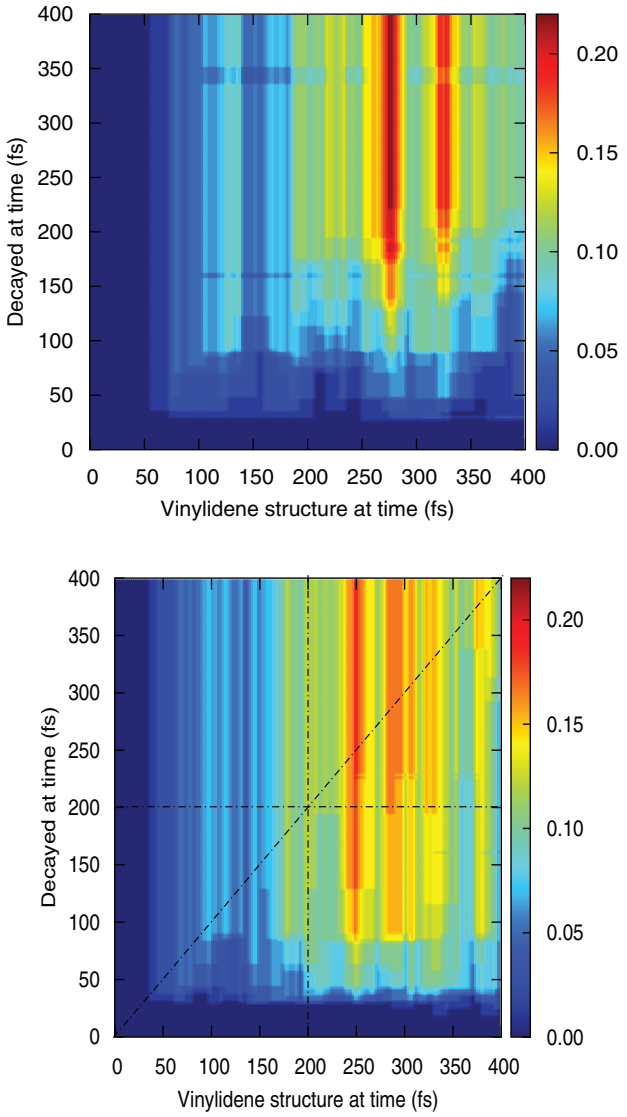

FIG. 6. Correlation function between the electronic decay and isomerization to vinylidene events (Eq. (3.3)) computed at two different sampling temperatures using FSSH method. Upper part for T = 10 K and lower part for T = 100 K. The horizontal line on the lower part of the figure corresponds to all trajectories that had decayed at or before 200 fs. Following it from left to right one sees the fraction of trajectories that are formed in vinylidene-like structures. In this way we can follow the isomerization dynamics and identify clearly the recurrence effects. The vertical line corresponds to isomerization events at 200 fs. We should note that not all trajectories which undergo isomerization stay in vinylidene-like structures but some may return back to acetylene-like structures. There are no recurrences in the vertical direction indicating that in this case the electronic decay is irreversible. If we take a point along the diagonal line and follow it in the vertical direction the correlation function remains constant. This indicates that the electronic decay process always occurs before isomerization.

perpendicular to it. The ensemble averaged of the correlation function between the electronic decay and isomerization is given by

$$C(t, t') = \langle g_{\mathrm{ed}}(t) g_{\mathrm{iso}}(t') \rangle. \tag{3.3}$$

The correlation function $C(t, t')$ computed using the FSSH algorithm and at two different sampling temperatures is shown in Figure 6. The upper part represents the FSSH results for T = 10 K and those for T = 100 K are given in the lower

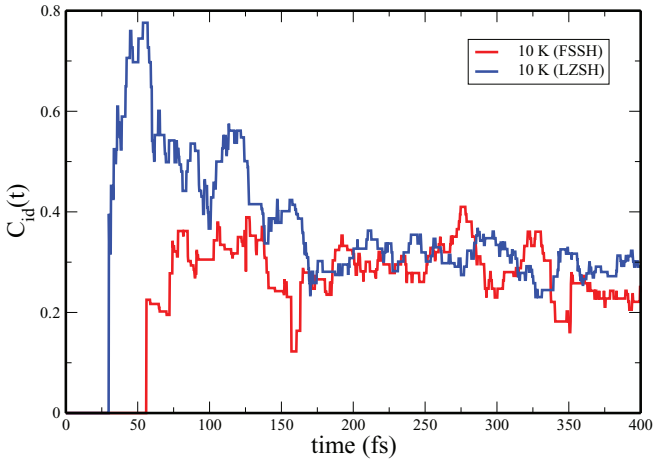

FIG. 7. Time evolution of the correlation function between the electronic decay and the isomerization process from acetylene to vinylidene (Eq. (3.4)) computed at T = 10 K using LZSH and FSSH algorithms.

part. Several informations can be read from the 2D maps in Figure 6. First of all, if the two events would be uncorrelated, the $C(t, t')$ function could be factorized as $\langle g_{ed}(t) g_{iso}(t')\rangle = \langle g_{ed}(t)\rangle \langle g_{iso}(t')\rangle$. It is clear that $C(t, t')$ cannot be factorized in this way. Second, once the electronic decay to lower states has taken place as shown in Figure 6 the system remains in the ground state. This is clearly seen by inspecting the vertical continuous bars on the 2D map in Figure 6. Third, when looking at the 2D map along the horizontal isomerization time, the recurrences between acetylene and vinylidene can be clearly appreciated. These recurrences have a period of 50–75 fs, indicating a hydrogen migration time (between both carbons) of about 25–35 fs. For both sets of initial conditions, the electronic decay happens first and then isomerization follows. To support this observation, we have performed a set of calculations without allowing for electronic transitions which forbids relaxation of the electronic energy into vibrational energy. In this case no isomerization process was found and the monocation remains in acetylene-like structures. This means that the isomerization process is always preceded by electronic decay. This observation can be understood also by looking to the hydrogen migration path shown in Figure 3. We have also performed a set of calculations based on FSSH and starting from D_1 state and no isomerization process was found. The reason for that is also trivial because when starting from the state D_1 the molecule does not have enough energy to overcome the barrier and evolve to the trans-bent structure (see Figure 2). Let us now concentrate on the comparison between LZSH and FSSH. We define the following correlation function between the electronic decay and isomerization process at a particular time t:

$$C_{id}(t) = \frac{\langle g_{ed}(t) g_{iso}(t)\rangle - \langle g_{ed}(t)\rangle \langle g_{iso}(t)\rangle}{\sqrt{\langle g_{ed}^2(t)\rangle \langle g_{iso}^2(t)\rangle}}. \quad (3.4)$$

Figure 7 presents the time evolution of the correlation function $C_{id}(t)$. This correlation function will average to zero only if electronic decay and isomerization are independent events at time t. The correlation in the LZSH model starts already in the first 30 fs and increases rapidly to reach a maximum at around 60 fs. Therefore, in the first 100 fs, the simulation based on the LZSH shows strong correlation. This is a reflection of the fact that with the LZSH method most of the trajectories undergo isomerization shortly after the decay to the ground state. The correlation computed with the FSSH method starts just after 50 fs but the peak is less pronounced than when using LZSH method. The reason for this is that in the FSSH method and after the decay to the ground state, it turns out that different trajectories undergo isomerization at different times.

At longer times, the correlation function computed in the FSSH method shows similar behavior than the one computed in the LZSH method. This is because at long times for the LZSH case a fraction of trajectories, which are quickly isomerized after the decay, have returned to acetylene. This fraction is similar for both methods and leads to a similar asymptotic correlation, although the dynamics immediately after the decay was rather different.

In the following we further illustrate the different features of the LZSH and FSSH methods and provide further physical insight on the dynamics of $C_2H_2^+$ based on observations of some representative individual trajectories.

Figure 8(a) illustrates the time evolution of the PESs of the three first states of the monocation computed with the LZSH method for a selected trajectory. The two snapshots represent the structure of the monocation at the decay and isomerization times. The time evolution of the molecular structure along the corresponding trajectories simulated using LZSH and FSSH methods is given in Videos 1 and 2. For this trajectory, the decay of the D_2 state to the ground state occurs near a strong coupling region ($t = 38$ fs) at the minimum energy gap between D_2 and D_1 where the acetylene cation undergoes nonradiative transition back to the ground state. The decrease of the energy gap between D_2 and D_1 states is mainly due to the increase of the ground state (D_1) energy and not to the decrease of the excited state (D_2) state. In the first 40 fs, a rapid decrease in the energy gap is seen as the acetylene cation moves away from the linear structure to the trans-bent geometry. At the switching time, the monocation has a trans-bent structure as shown in the first snapshot. Shortly after the decay, the molecule has already evolved to vinylidene structure at $t = 49$ as seen in the second snapshot. For this trajectory, the isomerization occurred just 10 fs after the decay to the ground state. After the transition to D_0, the trajectory remains on it for the rest of the simulation time.

In Figure 8(b), we consider the same trajectory (same initial conditions for position and velocities) as those used in Figure 8(a) but instead the FSSH is used. Now, the D_2 decays to D_1 after 46 fs, not so different from the time computed with the LZSH method. But now it takes longer time for the trajectory to undergo isomerization. In fact and for this trajectory, the isomerization process took place 140 fs after the decay of D_2 excited state to the D_1 state. The reason is probably that in the FSSH calculation this trajectory had already passed the seam region when it decayed and it was not moving any more in the direction of vinylidene. The presence of this kind of trajectories is what contributes to a reduced correlation in Figure 7. Let us now try to explain the reasons for the

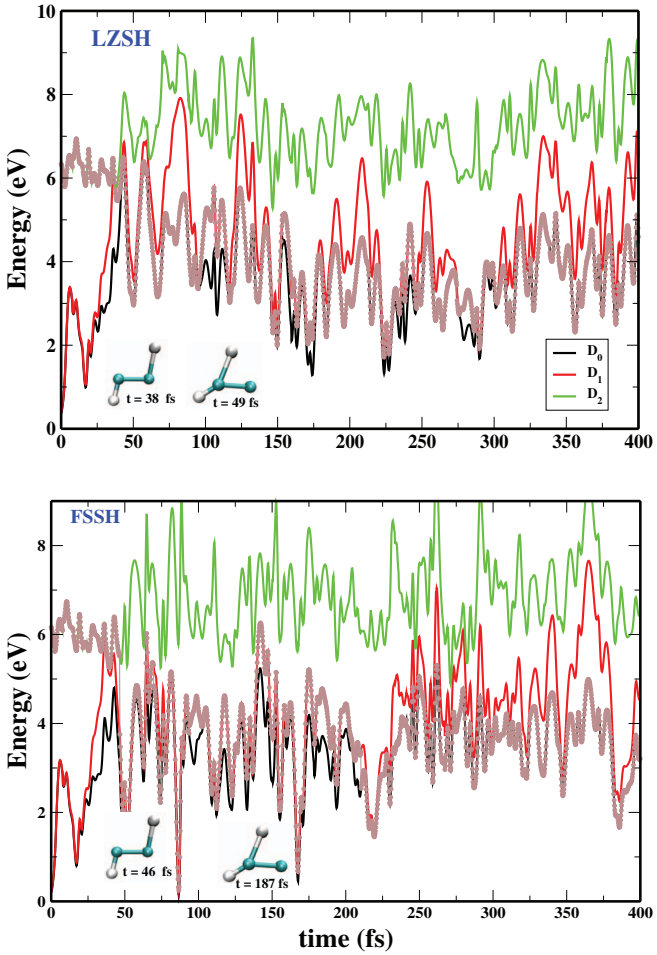

FIG. 8. Time evolution of the potential energy surfaces for the three states of acetylene monocation for an illustrative trajectory selected from the simulation, started in the first excited state (D_2), computed using LZSH and FSSH algorithms. The propagated state is given by brown circles. The snapshots correspond to the structure at the time of the electronic decay and at the isomerization time, respectively. For the complete time evolution of molecular structure computed using LZSH and FSSH see Videos 1 and 2 (enhanced online). [URL: http://dx.doi.org/10.1063/1.4793215.1] [URL: http://dx.doi.org/10.1063/1.4793215.2]

discrepancies between the results based on LZSH and FSSH methods. It is evident that those differences are due to different ways used in both algorithms for computing the transition probabilities.

In the LZSH method, the transition probability is computed at the minimum energy gap between the two PESs. Consequently, the hopping tends to occur close or at the minimum energy point on the conical intersection seam and nearly most of the trajectories hop coherently to the lower PES. In this case, the switch is driven in the direction of the momentum components which leads to the decay in vinylidene-like structures. This is reflected by a fast increase of the correlation function computed with LZSH and plotted in Figure 7. Contrary to LZSH, in the FSSH method trajectories can hop to a lower electronic state before or after the crossing region is reached. Since the FSSH is based on a continuous estimation of hopping probabilities based on the solution of the TDSE for the electronic subsystem, it probably provides a description closer to the real physical process as the LZSH, which leads to overestimation of the correlation between both decay and isomerization. Those transitions that can take place before or after the conical intersection seam, drive the molecule to relax to the ground state of the acetylene monocation with a higher probability (as can be seen clearly in Figure 3). The excited molecule spends some time in the acetylene-like structures and has enough energy to climb up the barrier and evolve to vinylidene-like structures. This is why the isomerization process is delayed when using FSSH method.

Based on the above observations it seems plausible that by dumping the electronic population from the excited state to the ground state at a well defined time, the isomerization process could be suppressed. This process could be achieved, for example, by applying an external laser field that could lead to the possibility of controlling the dynamics by reducing or enhancing the isomerization process. It is already known that coherent control techniques are usually used to actively manipulate the outcome of chemical reactions and thereby controlling the structural changes of the molecule. Those techniques are of great interest in chemical dynamics. Recently, Prokhorenko *et al.*[56] have used a weak-field coherent control approach to experimentally manipulate the isomerization yield of retinal in bacteriorhodopsin. They showed that the absolute quantity of 13-cis can be enhanced or suppressed. As an extension of the present study, we are already working on including external fields explicitly in the dynamics calculations and will investigate for which parameters of the field the isomerization can be enhanced or suppressed.

IV. CONCLUSION

We provide a detailed study of the interplay between non-radiative electronic decay and hydrogen migration in acetylene monocation after ionization into the $A^2\Sigma_g^+$ electronic state. The PES and NAC are computed at the CASSCF level of theory, and the dynamics is treated by TSH. The photoionization of acetylene into the first excited state drives the molecule from the linear structure to a trans-bent molecular configuration. Through a conical intersection it can relax back to either the ground state of acetylene or vinylidene-like structures. Based on the analysis of correlation functions we identify coherent motion between acetylene and vinylidene structures after the electronic non-radiative decay, which persists well up to 400 fs and has a period of about 50–75 fs. This is a classical effect in which many trajectories evolve coherently and have not yet dephased from one another. We find that both LZSH and FSSH algorithms lead to similar electronic population decay. Besides some differences in the time scales which we discuss and explain, LZSH and FSSH lead practically to the same physical picture of the dynamics. In both TSH methods, the isomerization is preceded by electronic decay and the sampling of initial conditions at different sampling temperatures does not qualitatively affect the results. Our simulations pave the way to achieve active control of the isomerization process in acetylene by inducing electronic transition at well defined times.

ACKNOWLEDGMENTS

We acknowledge S.-K. Son and R. Santra for careful reading of the manuscript and useful discussions.

[1]T. Osipov, C. L. Cocke, M. H. Prior, A. Landers, Th. Weber, O. Jagutzki, L. Schimdt, H. Schmidt-Böcking, and R. Dörner, Phys. Rev. Lett. **90**, 233002 (2003).
[2]A. Hishikawa, A. Matsuda, M. Fushitani, and E. J. Takahashi, Phys. Rev. Lett. **99**, 258302 (2007).
[3]Y. H. Jiang, A. Rudenko, O. Herrwerth, L. Foucar, M. Kurka, K. U. Kühnel, M. F. Kling, J. van Tilborg, A. Belkacem, K. Ueda, S. Düsterer, R. Treusch, C. D. Schröter, R. Moshammer, and J. Ullrich, Phys. Rev. Lett. **105**, 263002 (2010).
[4]Ch. Cha, R. Weinkauf, and U. Boesl, J. Chem. Phys. **103**, 5224 (1995).
[5]P. Rosmus, P. Botschwina, and J. P. Maier, Chem. Phys. Lett. **84**, 71 (1981).
[6]R. C. Gillen, B. Ostojic, and W. Domcke, Chem. Phys. **272**, 1 (2001).
[7]M. E. Madjet, O. Vendrell, and R. Santra, Phys. Rev. Lett. **107**, 263002 (2011).
[8]G. A. Worth and L. S. Cederbaum, Annu. Rev. Phys. Chem. **55**, 127 (2004).
[9]P. Ehrenfest, Z. Phys. **45**, 455 (1927).
[10]J. C. Tully and P. K. Preston, J. Chem. Phys. **55**, 562 (1971).
[11]M. Barbatti and H. Lischka, J. Am. Chem. Soc. **130**, 6831 (2008).
[12]E. Tapavicza, I. Tavernelli, U. Rothlisberger, C. Filippi, and M. E. Casida, J. Chem. Phys. **129**, 124108 (2008).
[13]A. I. Voronin, J. M. C. Marques, and A. J. C. Varandas, J. Phys. Chem. A **102**, 6057 (1998).
[14]C. F. Craig, W. R. Duncan, and O. V. Prezhdo, Phys. Rev. Lett. **95**, 163001 (2005).
[15]R. Mitrić, U. Werner, and V. Bonacić-Koutecký, J. Chem. Phys. **129**, 164118 (2008).
[16]J. C. Tully, J. Chem. Phys. **93**, 1061 (1990).
[17]E. Tapavicza, I. Tavernelli, and U. Rothlisberger, Phys. Rev. Lett. **98**, 023001 (2007).
[18]L. D. Landau, Phys. Z. Sowjetunion **2**, 46 (1932).
[19]C. Zener, Proc. R. Soc. London, Ser. A **137**, 696 (1932).
[20]G. Granucci, M. Persico, and A. Zoccante, J. Chem. Phys. **133**, 134111 (2010).
[21]J. E. Subotnik and N. Shenvi, J. Chem. Phys. **134**, 024105 (2011).
[22]B. R. Landry and J. E. Subotnik, J. Phys. Chem. **137**, 22A513 (2012).
[23]G. A. Worth, P. Hunt, and M. A. Robb, J. Phys. Chem. A **107**, 621 (2003).
[24]W. C. Swope, H. C. Andersen, P. H. Berens, and K. R. Wilson, J. Chem. Phys. **76**, 637 (1982).
[25]S. Hammes-Schiffer and J. C. Tully, J. Chem. Phys. **101**, 4657 (1994).
[26]J. Pittner, H. Lischka, and M. Barbatti, Chem. Phys. **356**, 147 (2009).
[27]E. Fabiano, T. W. Keal, and W. Thiel, Chem. Phys. **349**, 334 (2008).
[28]M. Barbatti, G. Granucci, M. Persico, M. Ruckenbauer, M. Vazdar, M. Eckert-Maksic, and H. Lischka, J. Photochem. Photobiol. A **190**, 228 (2007).
[29]U. Werner, R. Mitric, T. Suzuki, and V. Bonacic-Koutecky, Chem. Phys. **349**, 319 (2008).
[30]M. Barbatii, WIRES: Comput. Mol. Sci. **1**, 620 (2011).
[31]C. Wittig, J. Phys. Chem. B **109**, 8428 (2005).
[32]G. A. Jones, B. K. Carpenter, and M. N. Paddon-Row, J. Am. Chem. Soc. **120**, 5499 (1998).
[33]W. H. Miller and T. F. George, J. Chem. Phys. **56**, 5637 (1972).
[34]M. S. Topaler *et al*., J. Phys. Chem. A **102**, 1666 (1998).
[35]T. Nelson, S. Fernadez-Alberti, V. Chernyak, A. E. Roitberg, and S. Tretiak, J. Chem. Phys. **136**, 054108 (2012).
[36]M. C. Wells and R. R. Lucchese, J. Chem. Phys. **111**, 6290 (1999).
[37]G. Fronzoni, M. Stener, and P. Decleva, Chem. Phys. **298**, 141 (2004).
[38]N. Douguet, T. N. Rescigno, and A. E. Orel, Phys. Rev. A **86**, 013425 (2012).
[39]G. Cooper, T. Ibuki, Y. Iida, and C. E. Brion, Chem. Phys. **125**, 307 (1988).
[40]R. A. Mackie, S. W. J. Scully, A. M. Sands, R. Browning, K. F. Dunn, and C. J. Latimer, Int. J. Mass Spectrom. **223**, 67 (2003).
[41]O. Vendrell, Z. Li, and M. E. Madjet, Quantum Dynamics Tool Kit for quantum and surface hopping dynamics, Revision 269, DESY, Hamburg, Germany, 2012.
[42]F. Aquilante, L. De Vico, N. Ferré, G. Ghigo, P-.A. Malmqvist, T. Pedersen, M. Pitonak, M. Reiher, B. O. Roos, L. Serrano-Andrés, M. Urban, V. Veryazov, and R. Lindh, J. Comput. Chem. **31**, 224 (2010).
[43]B. J. Smith, R. Smernik, and L. Radom, Chem. Phys. Lett. **188**, 589 (1992).
[44]W. P. Kraemer and W. Koch, Chem. Phys. Lett. **212**, 631 (1993).
[45]G. Chambaud, R. Van den Boom, and P. Rosmus, Chem Phys. Lett. **247**, 79 (1995).
[46]M. Peric, B. Engels, and M. Hanrath, Chem. Phys. **238**, 33 (1998).
[47]K. Malsch, R. Rebentisch, P. Swiderek, and G. Hohlneicker, Theor. Chem. Acc. **100**, 171 (1998).
[48]B. S. Jursic, Int. J. Quant. Chem. **72**, 571 (1999).
[49]S. Zou and J. M. Bowman, Chem. Phys. Lett. **368**, 421 (2003).
[50]J. Pitarch-Ruiz, J. Sánchez-Marín, and D. Maynau, J. Comput. Chem. **24**, 609 (2003).
[51]T. S. Zyubina, Y. A. Dyakov, S. H. Lin, A. D. Bandrauk, and A. M. Mebel, J. Chem. Phys. **123**, 134320 (2005).
[52]S. Boyé-Péronne, D. Gauyacq, and J. Liévin, J. Chem. Phys. **124**, 214305 (2006).
[53]M. Peric, B. Ostojic, and B. Engels, J. Chem. Phys. **109**, 3086 (1998).
[54]M Kaledin, A. L. Kaledin, and J. M. Bowman, J. Phys. Chem. A **110**, 2933 (2006).
[55]W. H. Miller, J. Chem. Phys. **136**, 210901 (2012).
[56]V. I. Prokhorenko, A. M. Nagy, S. A. Waschuk, L. S. Brown, R. R. Birg, and R. J. D. Miller, Science **313**, 1257 (2006).